RSC Advances

ROYAL SOCIETY OF CHEMISTRY

PAPER

View Article Online
View Journal | View Issue

Check for updates

Cite this: RSC Adv., 2020, 10, 11493

Polymorphism of $Au_{11}(PR_3)_7Cl_3$ clusters: understanding C–H⋯π interaction and C–H⋯Cl–C van der Waals interaction on cluster assembly by surface modification†

Chenwanli Qin,[ab] Qianqin Yuan,[ab] Peng Li, *[ab] Shuxin Wang, [ab] Shuang Chen*[abc] and Manzhou Zhu *[ab]

The C–H⋯π interaction and the C–H⋯Cl–C van der Waals interaction play a crucial role in the crystallization of nanoclusters. In this paper, we present an example of a crystal system transformation of $Au_{11}(PR_3)_7Cl_3$ from monoclinic (M) to trigonal (T) by surface modification. Atomically-resolved gold nanoclusters containing tris(4-chlorophenyl)phosphine and chloride ligands were synthesized and determined to be $Au_{11}(p\text{-ClPPh}_3)_7Cl_3$ (p-ClPPh$_3$ = tris(4-chlorophenyl)phosphine) by X-ray crystallography. Crystal data demonstrated that the C–H⋯Cl–C interaction is dominant in a trigonal crystal system of $Au_{11}(p\text{-ClPPh}_3)_7Cl_3$ with a $R\bar{3}$ space group. However, the C–H⋯π interaction is the major driving force to form a monoclinic crystal system of $Au_{11}(PPh_3)_7Cl_3$ (PPh_3 = triphenylphosphine) with a $P2(1)/n$ space group. Moreover, UV-vis absorption spectra and X-ray photoelectron spectra reveal that the electronic structure of the $Au_{11}(p\text{-ClPPh}_3)_7Cl_3$ nanocluster is greatly influenced by p-ClPPh$_3$. This work provides critical implications for the crystallization of metal nanoclusters, as well as a better understanding of the non-covalent interaction on the nanocluster assembly and the crystal engineering by surface modification.

Received 10th February 2020
Accepted 9th March 2020

DOI: 10.1039/d0ra01288b

rsc.li/rsc-advances

Introduction

Atomically precise noble metal nanoclusters have received widespread attention due to their peculiar applications, such as catalysis, energy conversion, and biomedicine.[1–6] Recently, experimental and theoretical studies of metal nanoclusters have witnessed tremendous progress. More importantly, the structure of these nanoclusters can be identified by single-crystal X-ray diffraction (SC-XRD).[7–10] Based on this advantage, it is possible to probe the structure details and the structure-related properties at the atomic level, which is highly desirable to further practical applications.[11–13]

Ligands play a crucial role in the stabilization of nanoclusters.[14–17] The non-covalent interactions between surface ligands not only alter properties of clusters but also have significant effects on nanocluster assembly and self-assembly.[18–30] For instance, Wu and co-workers demonstrated that C–H⋯π interactions facilitated the chiral arrangement of ligands, and the assembled ligands presented rotational and parallel patterns on the surface of the nanoparticles.[14] Pradeep and colleagues reported that C–H⋯π interactions are dominant in a cubic lattice and result in a higher luminescence efficiency.[16] Crudden *et al.* showed that multiple C–H⋯π and π⋯π interactions rigidify the ligands and contribute to the high photoluminescent quantum yields in the Au_{13} nanocluster.[31] Zheng *et al.* reported that π⋯π interactions play a crucial role in stabilizing silver nanoclusters.[32] Xie *et al.* found that the assembly behaviour of clusters can be regulated by metal ions (*i.e.*, Ag^+/Cs^+).[33] Non-covalent interactions play an important role in nanocluster chemistry.[34,35] To date, a series of $Au_{11}(PR_3)Cl_3$ nanoclusters with adjustable ligands have been extensively studied comparing with other nanoclusters.[15,36–39] Therefore, $Au_{11}(PR_3)Cl_3$ clusters are chosen as models to investigate non-covalent interactions in the crystallization of nanoclusters by surface modification.

In the following, we synthesized $Au_{11}(p\text{-ClPPh}_3)_7Cl_3$ (**Au_{11}-Cl** for short) and $Au_{11}(PPh_3)_7Cl_3$ (**Au_{11}-H** for short) nanoclusters by using tris(4-chlorophenyl)phosphine and triphenylphosphine as the protecting ligand. The composition of the **Au_{11}-Cl** was

[a] *Department of Chemistry and Centre for Atomic Engineering of Advanced Materials, Anhui Province Key Laboratory of Chemistry for Inorganic/Organic Hybrid Functionalized Materials, Anhui University, Hefei, Anhui, 230601, P. R. China. E-mail: peng-li@ahu.edu.cn; chenshuang@ahu.edu.cn; zmz@ahu.edu.cn*

[b] *Key Laboratory of Structure and Functional Regulation of Hybrid Materials, Anhui University, Ministry of Education, Hefei, 230601, P. R. China*

[c] *Institutes of Physical Science and Information Technology, Anhui University, Hefei, Anhui, 230601, P. R. China*

† Electronic supplementary information (ESI) available. CCDC 1966633. For ESI and crystallographic data in CIF or other electronic format see DOI: 10.1039/d0ra01288b

characterized by electron spin ionization (ESI-MS), and the structure of the **Au_{11}-Cl** was determined by X-ray crystallography. We are engaged in illuminating the crystal system transformation ascribed to C–H⋯Cl–C interactions and C–H⋯π interactions. The different patterns of non-covalent interactions can alter the packing of nanoclusters into monoclinic or trigonal lattice. The distance between H and H atom (D_{HH} for short) reveals the non-covalent interactions of the intramolecular can also be changed through surface modification. Furthermore, UV-vis absorption spectra and X-ray photoelectron spectra reveal the difference in the electronic structure due to surface modification.

Experimental

Chemicals

All chemicals are commercial and were used without further purification. Hydrogen tetrachloroaurate tetrahydrate ($HAuCl_4 \cdot 4H_2O$, 99.95%), triphenylphosphine (PPh_3, 98%), tris(4-chlorophenyl)phosphine (*p*-$ClPPh_3$, 98%), sodium borohydride ($NaBH_4$, 99.99%), methanol (HPLC grade, 99.9%) methylene chloride (HPLC grade, 99.9%), hexane (HPLC grade, 99.9%), ethanol (HPLC grade, 99.9%). Ultrapure water was purchased from Wahaha Co. Ltd. All glassware was cleaned with aqua regia (3 : 1 mix of hydrochloric acid and nitric acid), rinsed with ultrapure water, and then dried before use.

Synthesis of Au_{11}(*p*-$ClPPh_3$)$_7$$Cl_3$ (Au_{11}-Cl) and crystallization

First, $HAuCl_4 \cdot 4H_2O$ (157 mg, 0.4 mmol) was dissolved in 15 mL ethanol, tris(4-chlorophenyl)phosphine (0.15 g, 0.5 mmol) was dissolved in the solution. The solution was stirred (∼1200 rpm) in a 50 mL round bottom flask. After stirring for 20 min, the solution colour turned turbid. Then, 5 mL ethanol solution of $NaBH_4$ (40 mg) was added, and the colour of solution changed from turbid to dark immediately. After stirring for 8 h, the organic solution was evaporated and washed several times with hexane to remove the redundant phosphine and other by-products. Finally, The **Au_{11}-Cl** nanocluster was crystallized in vapour diffusion of hexane/CH_2Cl_2 at room temperature.

Synthesis of $Au_{11}(PPh_3)_7Cl_3$ (Au_{11}-H)

The $Au_{11}(PPh_3)_7Cl_3$ was synthesized according to the method in the literature by Hutchison *et al.*[36] First, $AuCl(PPh_3)$ (500 mg) was dissolved in 15 mL ethanol solution and $NaBH_4$ (190 mg, 5 mmol dissolved) was slowly added to the solution. After stirring for 8 h, the organic solution was evaporated and washed several times with hexane to remove the excess PPh_3 and other by-products. The pure **Au_{11}-H** was red solid and crystallized in vapour diffusion of hexane/CH_2Cl_2 at room temperature.

Characterization

UV-vis spectra of nanoclusters in CH_2Cl_2 were performed on the UV-6000PC instrument.

Red-brown crystals were collected, and the structure of **Au_{11}-Cl** was determined by X-ray crystallography. Single crystal X-ray diffraction data of the **Au_{11}-Cl** was collected on a Bruker Smart 1000 CCD. The area detector used graphite-monochromatized Mo Kα radiation ($\lambda = 0.71069$ Å). A piece of red-brown block-shaped crystal (0.25 × 0.24 × 0.23 mm) was mounted onto a MiTeGen capillary with Fluorolube, and all structures were solved by direct methods using SHELXS-97. Data collection was performed under room temperature (296 K).

The electrospray ionization time-of-flight mass spectrometry (ESI-TOF-MS) measurement was recorded using UPLC H-Class XEVO G2 XS Qtof (Waters. Crop.). The **Au_{11}-Cl** was recorded in the positive ion mode when dissolving in CH_3OH, containing 50 mM CsOAc, and centrifugation for 5 min (12 000 rpm). The sample was infused at 180 μL h^{-1}. The source temperature was kept at 50 °C with the spray voltage keeping at 4 kV. The mass spectra were processed using Masslynx 4.1 software (Waters Corp.).

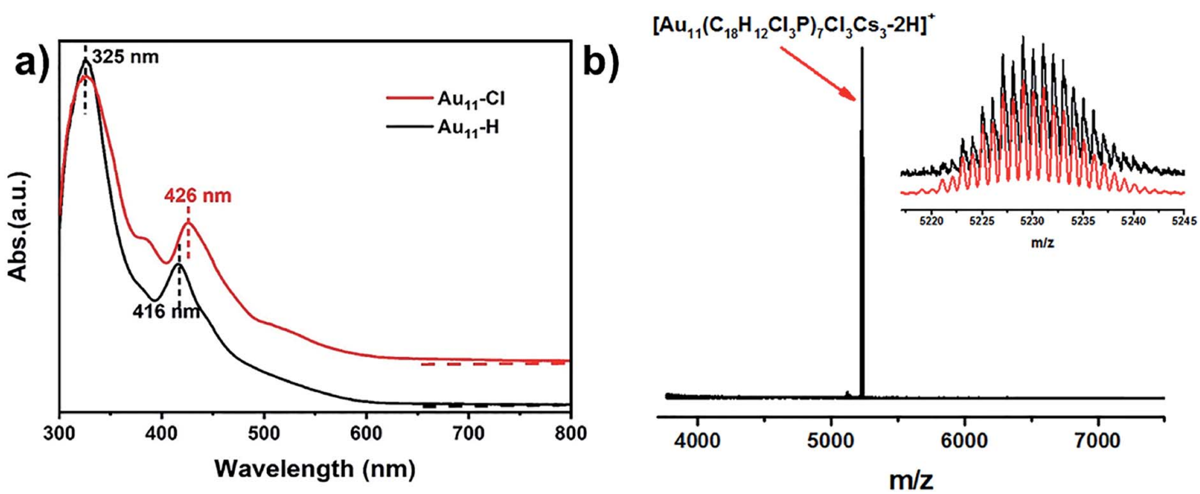

Fig. 1 (a) The UV-vis absorption spectra of **Au_{11}-Cl** and **Au_{11}-H**. (b) Positive ion mode ESI-TOF-MS of **Au_{11}-Cl** clusters in CH_3OH, inset: overlap of the experimental data (black) and the simulated spectrum (red) for **Au_{11}-Cl**.

The Thermo ESCALAB 250 instrument was used to measure X-ray photoelectron spectroscopy (XPS), which configured with a monochromated Al Kα (1486.8 eV) 150 W X-ray source, 0.5 mm circular spot size, and the analysis chamber base pressure lower than 1×10^{-9} mbar. Data were collected with FAT = 20 eV.

Results and discussions

As shown in Fig. 1a, the ultraviolet-visible (UV-vis) absorption spectrum of **Au_{11}-H** (black) shows two prominent peaks at 325 nm and 416 nm. While the UV-vis absorption spectrum of the **Au_{11}-Cl** (red) shows three peaks at 325 nm, 390 nm and 426 nm, respectively. The differences of absorption spectra possibly indicate that the electronic structure is distinctive, resulting from the replacement of PPh_3 by *p*-$ClPPh_3$. More, the thermodynamic stability of the Au_{11} was explored under room temperature (Fig. S1†). These results imply the **Au_{11}-H** is more stable than **Au_{11}-Cl**. The formula of **Au_{11}-Cl** was confirmed by electrospray ionization time-of-flight mass spectrometry (ESI-TOF-MS). As shown in Fig. 1b, the ESI-TOF-MS (positive ion mode) revealed a single intense peak at $m/z = 5230.02$ Da, and the 1 gap between isotopic peaks proves that $z = 1$. The formula is attributed to $[Au_{11}(C_{18}H_{12}Cl_3P)_7Cl_3Cs_3{-}2H]^+$ (**Au_{11}-Cl**). The experimental data matched well with the theoretical simulation indicates the purity of **Au_{11}-Cl**. X-ray photoelectron spectroscopy (XPS) was further performed to reveal the electronic structure of **Au_{11}-Cl** and **Au_{11}-H**. Fig. S2† shows the total spectra of XPS for two nanoclusters. The Au 4f peak (84.53 eV) of **Au_{11}-Cl** nanocluster is on the higher energy side compared to that of **Au_{11}-H** (84.05 eV), which means the Au atoms in the **Au_{11}-Cl** are more oxidized than those in the **Au_{11}-H**.

The structure of **Au_{11}-Cl** was determined by the single crystal X-ray crystallography (Fig. 2). The molecular structure of the **Au_{11}-Cl** is similar to that of the **Au_{11}-H**. Ten gold atoms (yellow) form an incomplete icosahedral structure with one gold atom in the centre. And the ligands of six *p*-$ClPPh_3$ (pink) and three Cl (green) atoms cap the metal core along the C_3 axis with one *p*-$ClPPh_3$ ligand on the C_3 axis. In comparison with the **Au_{11}-H**, the **Au_{11}-Cl** crystal possesses a larger cell volume (23 297.7 Å^3 *versus* 12 398 Å^3) and less density (2.066 g cm^{-3} *versus* 2.243 g cm^{-3}), which is possibly attributed to distinct non-covalent interactions in the unit cell. More comparisons of the cell details are given in Table S1.†

The packing of these two nanoclusters along (100), (010), and (001) planes is shown in Fig. 3, respectively. For the T system of **Au_{11}-Cl**, the nanoclusters are organized layer by layer with an fcc-like ABCABC style viewing along *a*-axis, *b*-axis, and *c*-axis (Fig. 3a–c). Especially, viewing along the *c*-axis, the **Au_{11}-Cl** gets organized into a hexagonal lattice, while the **Au_{11}-H** gets decorated into a rectangular lattice. In the case of the **Au_{11}-H**, the nanoclusters are packed layer by layer with an ABAB style viewing along the *a*-axis, *b*-axis, and *c*-axis (Fig. 3d–f). Although the **Au_{11}-Cl** and the **Au_{11}-H** are constructed with the same core structure, they display totally different lattices. The obvious

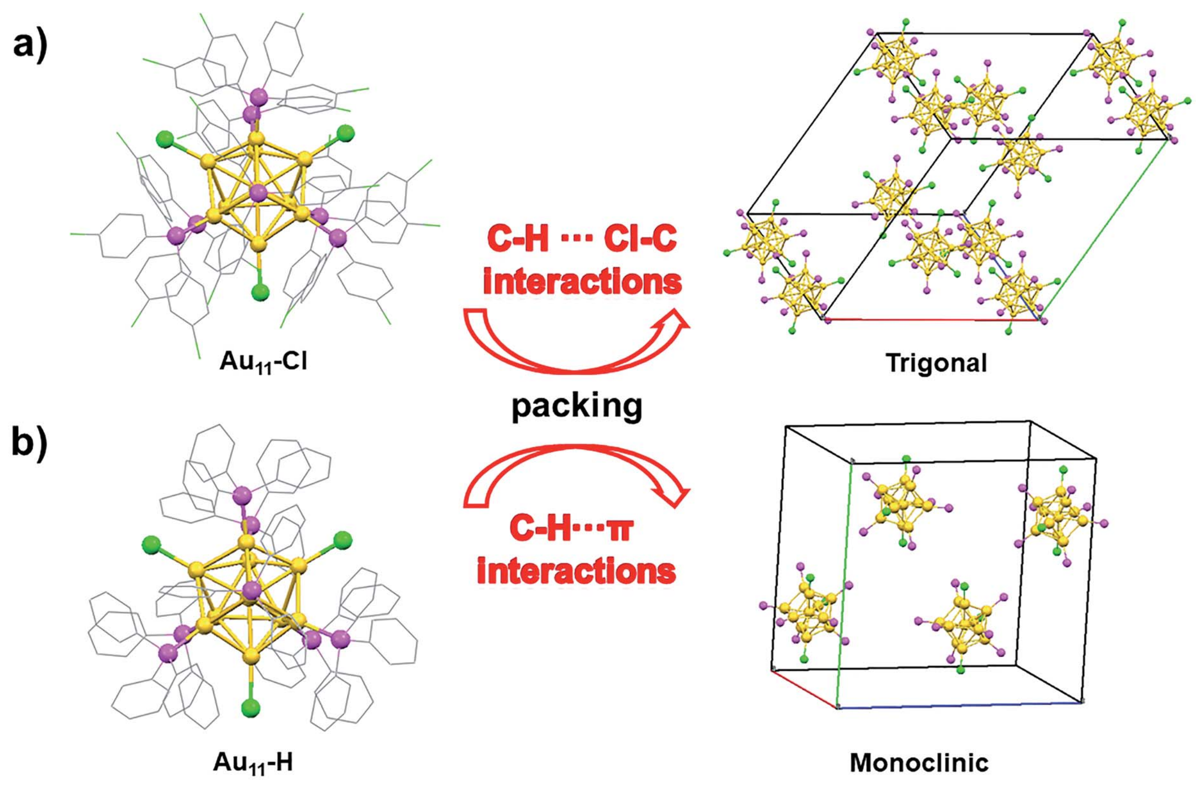

Fig. 2 (a) Crystal structure and trigonal unit cell of the Au_{11}-Cl. (b) Crystal structure and monoclinic unit of the Au_{11}-H. (colour labels: yellow = Au, pink = P, gray = C, green = Cl, for clarity all H atoms are not shown).

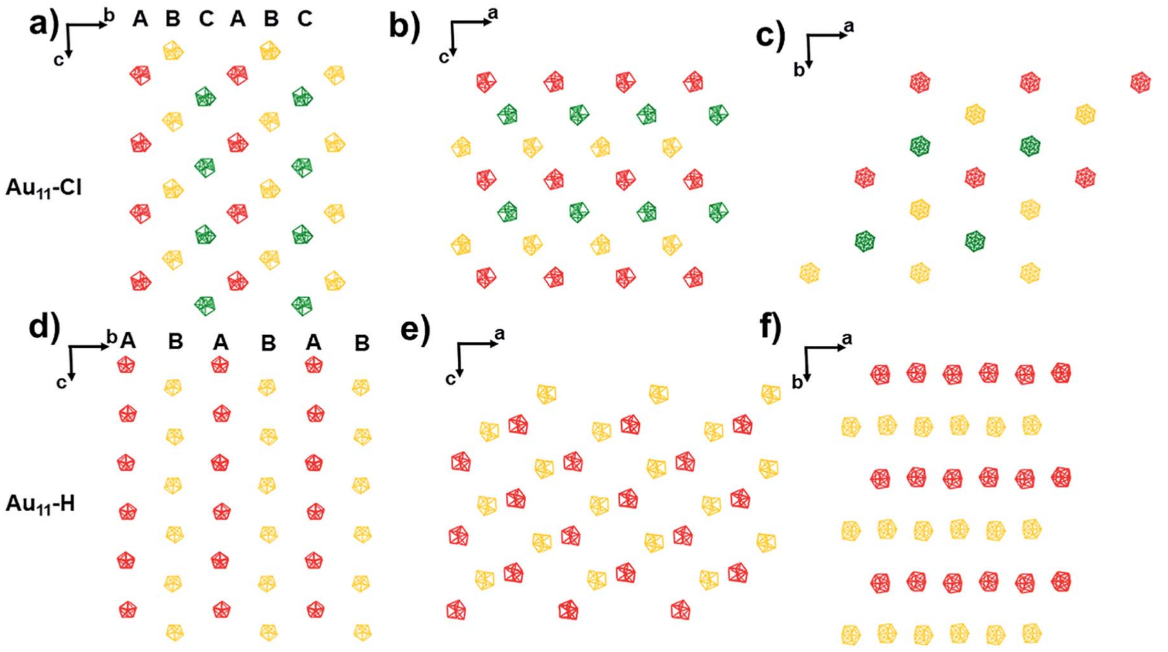

Fig. 3 Packing of the Au_{11}-H and the Au_{11}-Cl view from the (a and d) *a*-axis, (b and e) *b*-axis and (c and f) *c*-axis.

packing difference of the **Au_{11}** nanoclusters is related to the difference of non-covalent interactions between nanoclusters.[14]

C–H⋯π interactions play a crucial role in the crystal packing of the **Au_{11}-H**, which are the major driving force to form monoclinic. In the M system, each unit contains four **Au_{11}-H** nanoclusters. Fig. 4 shows the C–H⋯π interactions (red/blue dashed line) of the **Au_{11}-H**. C–H⋯π interactions exist between the C–H groups (blue) of the PPh_3 ligands and adjacent benzenes (green) of the adjacent cluster, evidenced by their distance. The distance of C–H⋯π ranges from 2.80 to 2.89 Å, with an average of 2.835 Å (Fig. S3†). Strong C–H⋯π interactions form a chain to hold each **Au_{11}-H** nanocluster and restrict the motion of the entire nanocluster.

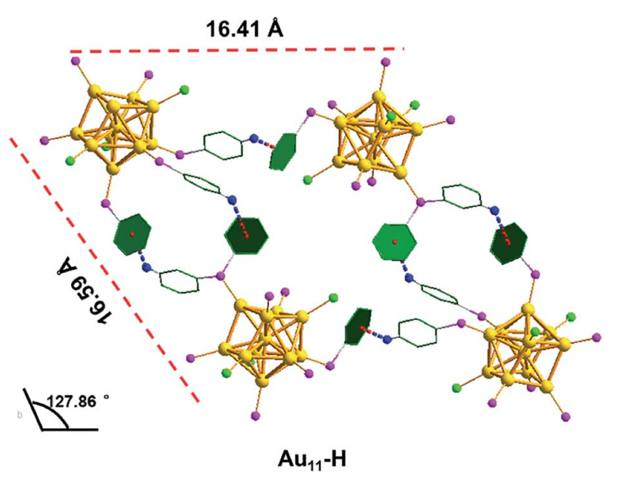

Fig. 4 The C–H⋯π interactions in the Au_{11}-H. Yellow = Au; pink = P; green = C; blue = H; bright green = Cl; blue red dashed, C–H⋯π interactions.

Interestingly, most H atoms form C–H⋯π interactions are located on the *para* position of the benzene rings in the **Au_{11}-H**, which inspires us to speculate whether these interactions could be destroyed by introducing an atom with a larger atomic radius in the *para* position. As we expected, by replacing PPh_3 with *p*-$ClPPh_3$ ligands that contain Cl atoms on the *para* position of aromatic rings, C–H⋯π interactions are not found in the unit cell of the as-obtained **Au_{11}-Cl**. In order to discuss the non-covalent interactions of **Au_{11}-Cl**, four **Au_{11}-Cl** clusters are marked by the green quadrilateral (Fig. S7†).

As shown in Fig. 5, the inter-cluster distances are 19.80 Å and 17.42 Å, respectively, and the corresponding obtuse is 125.42°. However, the lengths (16.41 Å and 16.59 Å) and obtuse (127.86°) of **Au_{11}-H** are different from those of **Au_{11}-Cl**. When zooming into the surfaces between nanoclusters, C–H⋯Cl–C

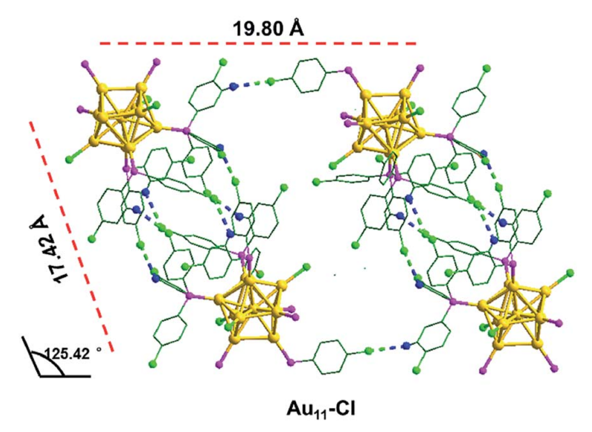

Fig. 5 The C–H⋯Cl–C interactions in the Au_{11}-Cl. Yellow = Au; pink = P; green = C; blue = H; bright green = Cl; bright green blue dashed, C–H⋯Cl–C interaction.

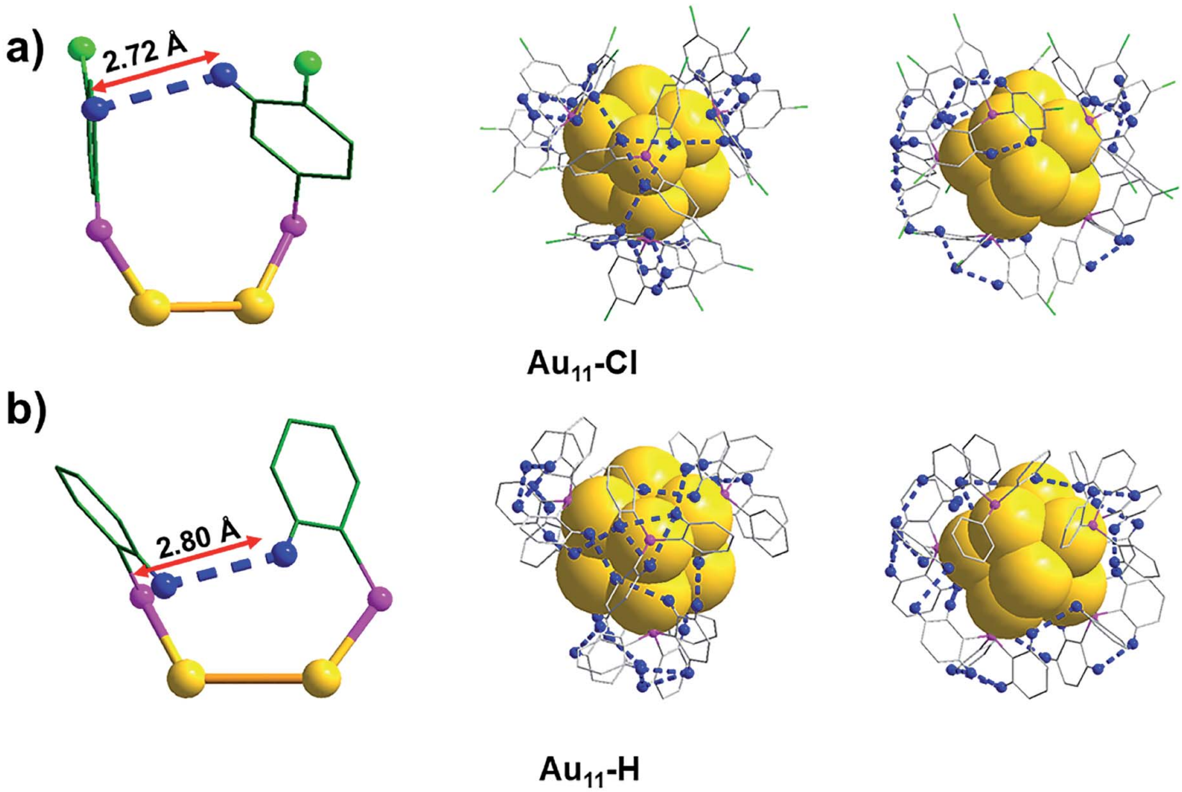

Fig. 6 The nearest neighbour H and H atoms in the intra-Au_{11}-Cl and intra-Au_{11}-H. (a) The nearest neighbour H and H atoms in the Au_{11}-Cl viewed from different angles. (b) The nearest neighbour H and H atoms in the Au_{11}-H viewed from different angles. Yellow = Au; pink = P; green = C; blue = H; bright green = Cl; blue dashed, intra-D_{HH}; for clarity other atoms are not shown.

interactions (bright green/blue dashed line) of the **Au_{11}-Cl** lead to form T systems in the unit. In the T lattice of **Au_{11}-Cl**, the average distance of the C–H⋯Cl–C interactions is 2.94 Å, with a range from 2.85 to 2.99 Å (Fig. S4†). This distance is consistent with the reported value.[40] Overall, comparing the C–H⋯Cl–C interactions and the C–H⋯π interactions suggests that the insertion of chlorine atoms breaks C–H⋯π interactions and changes the crystal system from M to T.

Another significant aspect is that the non-covalent interactions of the intra-molecular also changed because of the introduction of chlorine atoms in the surface ligands. The average distance of H and H (D_{HH} for short) in the **Au_{11}-Cl** is 2.72 Å (Fig. 6a and S5†). In contrast, the D_{HH} in the **Au_{11}-H** is 2.80 Å, varying from 2.53 to 2.99 Å (Fig. 6b and S6†), which is slightly larger than that of the **Au_{11}-Cl**. Viewing along the C_3 axis, the triangle constituted by nearest H atoms is slightly rotating compared with the one in **Au_{11}-Cl**, due to the introduction of the Cl atoms. The total numbers and average distances of the non-covalent interactions and the D_{HH} were shown in Table 1. All these results verify that non-covalent interactions of intra-cluster induce the rotation and arrangement of ligands, which further enable every single nanocluster to be compacted and ordered with reduced intra-cluster vibration, contributing to the formation of high-quality single crystals.

Table 1 The number of interactions for Au_{11}-Cl and Au_{11}-H

Interaction (distance)	**Au_{11}-H**	**Au_{11}-Cl**
CH⋯π	6 (2.84 Å)	×
C–H⋯Cl–C	×	20 (2.94 Å)
Inter-D_{HH}	46 (2.80 Å)	83 (2.81 Å)
Intra-D_{HH}	24 (2.79 Å)	21 (2.72 Å)

Conclusions

In summary, we have chosen the Au_{11}(*p*-$ClPPh_3$)$_7Cl_3$ (**Au_{11}-Cl**) and the $Au_{11}(PPh_3)_7Cl_3$ (**Au_{11}-H**) to investigate non-covalent interactions in the crystallization by surface modification. The chlorine atoms occupy the *para* of benzene rings in phosphine ligands, resulting in the breaking of C–H⋯π interactions and crystal system transformation. C–H⋯Cl–C interactions of Au_{11}(*p*-PPh_3)$_7Cl_3$ lead to the formation of trigonal systems, revealing the importance of the ligands on the non-covalent interaction modes. Moreover, UV-vis spectra and XPS spectra reveal the change of the electronic structure caused by surface modification. This work provides new insights into the effects of inter- and intra-interactions on nanocluster crystallization, making the assembly and self-assembly of metal nanoclusters more readily.

Conflicts of interest

There are no conflicts to declare.

Acknowledgements

We acknowledge financial support by NSFC (No. 21571001, 21372006, 21631001, and U1532141), the Ministry of Education, the Education Department of Anhui Province, and 211 Project of Anhui University.

Notes and references

1 R. Jin, C. Zeng, M. Zhou and Y. Chen, *Chem. Rev.*, 2016, **116**, 10346–10413.
2 I. Chakraborty and T. Pradeep, *Chem. Rev.*, 2017, **117**, 8208–8271.
3 J. Fang, B. Zhang, Q. Yao, Y. Yang, J. Xie and N. Yan, *Coord. Chem. Rev.*, 2016, **322**, 1–29.
4 H. Zhu, N. Goswami, Q. Yao, T. Chen, Y. Liu, Q. Xu, D. Chen, J. Lu and J. Xie, *J. Mater. Chem. A*, 2018, **6**, 1102–1108.
5 C. M. Aikens, *J. Phys. Chem. Lett.*, 2011, **2**, 99–104.
6 S. Xie, H. Tsunoyama, W. Kurashige, Y. Negishi and T. Tsukuda, *ACS Catal.*, 2012, **2**, 1519–1523.
7 M. Zhu, C. M. Aikens, F. J. Hollander, G. C. Schatz and R. Jin, *J. Am. Chem. Soc.*, 2008, **130**, 5883–5885.
8 P. D. Jadzinsky, G. Calero, C. J. Ackerson, D. A. Bushnell and R. D. Kornberg, *Science*, 2007, **318**, 430–433.
9 Y. Wang, X. K. Wan, L. Ren, H. Su, G. Li, S. Malola, S. Lin, Z. Tang, H. Hakkinen, B. K. Teo, Q. M. Wang and N. Zheng, *J. Am. Chem. Soc.*, 2016, **138**, 3278–3281.
10 C. P. Joshi, M. S. Bootharaju, M. J. Alhilaly and O. M. Bakr, *J. Am. Chem. Soc.*, 2015, **137**, 11578–11581.
11 Z. Wu, Q. Yao, S. Zang and J. Xie, *ACS Mater. Lett.*, 2019, **1**, 237–248.
12 M. Zhu, S. Jin and S. Wang, *Chem.–Asian J.*, 2019, **14**, 3222–3231.
13 R. W. Huang, Y. S. Wei, X. Y. Dong, X. H. Wu, C. X. Du, S. Q. Zang and T. C. W. Mak, *Nat. Chem.*, 2017, **9**, 689–697.
14 N. Yan, N. Xia, L. Liao, M. Zhu, F. Jin, R. Jin and Z. Wu, *Sci. Adv.*, 2018, **4**, eaat7259.
15 X. Kang, Y. Song, H. Deng, J. Zhang, B. Liu, C. Pan and M. Zhu, *RSC Adv.*, 2015, **5**, 66879–66885.
16 A. Nag, P. Chakraborty, M. Bodiuzzaman, T. Ahuja, S. Antharjanam and T. Pradeep, *Nanoscale*, 2018, **10**, 9851–9855.
17 S. Kumar and R. Jin, *Nanoscale*, 2012, **4**, 4222–4227.
18 P. Chakraborty, A. Nag, A. Chakraborty and T. Pradeep, *Acc. Chem. Res.*, 2019, **52**, 2–11.
19 P. Sun, Z. Wang, Y. Bi, D. Sun, T. Zhao, F. Zhao, W. Wang and X. Xin, *ACS Appl. Nano Mater.*, 2020, **3**, 2038–2046.
20 Z. Wu, J. Liu, Y. Gao, H. Liu, T. Li, H. Zou, Z. Wang, K. Zhang, Y. Wang, H. Zhang and B. Yang, *J. Am. Chem. Soc.*, 2015, **137**, 12906–12913.
21 Z. Wu, C. Dong, Y. Li, H. Hao, H. Zhang, Z. Lu and B. Yang, *Angew. Chem., Int. Ed.*, 2013, **52**, 9952–9955.
22 J. Fontana, W. J. Dressick, J. Phelps, J. E. Johnson, R. W. Rendell, T. Sampson, B. R. Ratna and C. M. Soto, *Small*, 2014, **10**, 3058–3063.
23 M. De Nardi, S. Antonello, D.-e. Jiang, F. Pan, K. Rissanen, M. Ruzzi, A. Venzo, A. Zoleo and F. Maran, *ACS Nano*, 2014, **8**, 8505–8512.
24 P. Chakraborty, A. Nag, G. Paramasivam, G. Natarajan and T. Pradeep, *ACS Nano*, 2018, **12**, 2415–2425.
25 V. Berry and R. F. Saraf, *Angew. Chem., Int. Ed.*, 2005, **44**, 6668–6673.
26 K. Müller-Dethlefs and P. Hobza, *Chem. Rev.*, 2000, **100**, 143–168.
27 Y. Song, S. Weng, H. Li, H. Yu and M. Zhu, *Inorg. Chem.*, 2019, **58**, 7136–7140.
28 S. Zhang, X. Lu, J. Sun, Y. Zhao and X. Shao, *CrystEngComm*, 2015, **17**, 4110–4116.
29 X. Kang and M. Zhu, *Coord. Chem. Rev.*, 2019, **394**, 1–38.
30 Z. Gan, J. Chen, J. Wang, C. Wang, M.-B. Li, C. Yao, S. Zhuang, A. Xu, L. Li and Z. Wu, *Nat. Commun.*, 2017, **8**, 14739.
31 M. R. Narouz, S. Takano, P. A. Lummis, T. I. Levchenko, A. Nazemi, S. Kaappa, S. Malola, G. Yousefalizadeh, L. A. Calhoun, K. G. Stamplecoskie, H. Hakkinen, T. Tsukuda and C. M. Crudden, *J. Am. Chem. Soc.*, 2019, **141**, 14997–15002.
32 H. Yang, Y. Wang, H. Huang, L. Gell, L. Lehtovaara, S. Malola, H. Hakkinen and N. Zheng, *Nat. Commun.*, 2013, **4**, 2422.
33 Q. Yao, Y. Yu, X. Yuan, Y. Yu, D. Zhao, J. Xie and J. Y. Lee, *Angew. Chem., Int. Ed.*, 2015, **54**, 184–189.
34 J. Liang, X.-S. Wu, X.-L. Wang, C. Qin, K.-Z. Shao, Z.-M. Su and R. Cao, *CrystEngComm*, 2016, **18**, 2327–2336.
35 J. Shen, Z. Wang, D. Sun, G. Liu, S. Yuan, M. Kurmoo and X. Xin, *Nanoscale*, 2017, **9**, 19191–19200.
36 L. C. McKenzie, T. O. Zaikova and J. E. Hutchison, *J. Am. Chem. Soc.*, 2014, **136**, 13426–13435.
37 Z. Qin, D. Zhao, L. Zhao, Q. Xiao, T. Wu, J. Zhang, C. Wan and G. Li, *Nanoscale Adv.*, 2019, **1**, 2529–2536.
38 Y. Shichibu, Y. Negishi, T. Tsukuda and T. Teranishi, *J. Am. Chem. Soc.*, 2005, **127**, 13464–13465.
39 M. R. Narouz, K. M. Osten, P. J. Unsworth, R. W. Y. Man, K. Salorinne, S. Takano, R. Tomihara, S. Kaappa, S. Malola, C. T. Dinh, J. D. Padmos, K. Ayoo, P. J. Garrett, M. Nambo, J. H. Horton, E. H. Sargent, H. Hakkinen, T. Tsukuda and C. M. Crudden, *Nat. Chem.*, 2019, **11**, 419–425.
40 P. K. Thallapally and A. Nangia, *CrystEngComm*, 2001, **3**, 114–119.

